

Selective optomechanically-induced amplification with driven oscillators

Tian-Xiang Lu,¹ Ya-Feng Jiao,¹ Hui-Lai Zhang,¹ Farhan Saif,² and Hui Jing^{1,*}

¹*Key Laboratory of Low-Dimensional Quantum Structures and Quantum Control of Ministry of Education, Department of Physics and Synergetic Innovation Center for Quantum Effects and Applications, Hunan Normal University, Changsha 410081, China*

²*Department of Electronics, Quaid-i-Azam University, 45320 Islamabad, Pakistan*

We study optomechanically-induced transparency (OMIT) in a compound system consisting of an optical cavity and an acoustic molecule, which features not only double OMIT peaks but also light advance. We find that by selectively driving one of the acoustic modes, OMIT peaks can be amplified either symmetrically or asymmetrically, accompanied by either significantly enhanced advance or a transition from advance to delay of the signal light. The sensitive impacts of the mechanical driving fields on the optical properties, including the signal transmission and its higher-order sidebands, are also revealed. Our results confirm that selective acoustic control of OMIT devices provides a versatile route to achieve multi-band optical modulations, weak-signal sensing, and coherent communications of light.

PACS numbers: 42.50.WK, 42.65.Hw, 03.65.Ta

I. INTRODUCTION

Cavity optomechanics (COM), focusing on the interplay of optical lasers and mechanical devices, provides unprecedented opportunities to explore both fundamental issues of quantum mechanics [1, 2] and practical quantum control of light and sound [3–16]. A prominent example, which is closely related to our present work, is optomechanically-induced transparency (OMIT) [17–20]. Playing a key role in COM-based coherent control of light, OMIT has been experimentally demonstrated with microtoroid resonators [20], diamond crystals [21], microwave circuits [22], nanobeam or membrane devices [23, 24], and nonlinear resonators [25, 26]. In recent works, more exotic properties of OMIT devices have been revealed, such as cascaded OMIT [27], nonreciprocal OMIT [28–31], reversed OMIT [32–34], vector OMIT [35], nonlinear OMIT [36–38], two-color OMIT [39], and sub-Hertz OMIT [40]. These devices provide a powerful platform to realize, for examples, quantum memory [23, 41, 42], signal sensing [43–47], and phononic engineering [48–51].

Very recently, COM devices fabricated with optical dimers (i.e., coupled optical resonators) [12, 52–55] or acoustic dimers [27, 56–60], have been utilized to achieve, for examples, COM-based phonon lasing [12–14], unconventional photon blockade [61–64], and topological COM control [53, 65, 66]. In particular, by using multi-mode mechanical elements, experimentalists have demonstrated phonon-phonon entanglement [59, 60], two-mode phonon laser [11], optomechanical Ising dynamics [67], mechanical synchronization or multi-wave phonon mixing [56, 57, 68], and coherent phonon transfer [69]. Appealing predictions for this system also include acoustic Josephson junctions [70], COM superradiance

[71, 72], parity-time symmetry acoustics [73], and phononic crystal shield [74].

In this paper, we focus on the role of selective mechanical pump in OMIT with two coupled mechanical resonators (MRs). In experiments, this three-mode COM system has been demonstrated with a double-microdisk resonator, a zipper nanobeam photonic crystal, or a microwave device with two micromechanical beams [56, 75]. Strong mechanical driving has also been utilized to achieve hybrid quantum spin-phonon devices [76] or ultra-strong exciton-phonon coupling [77]. In the absence of the mechanical driving, such a system features double OMIT spectrum, i.e., the appearance of two symmetric transparent peaks around an absorption dip at the cavity resonance (which is otherwise a transparent peak for COM with a single mechanical oscillator [20, 23]). Here we find that, by selectively driving the mechanical resonators, the OMIT peaks and the accompanied optical group delays can be significantly altered. In comparison with the case of only a single driven oscillator [78–84], in our system, we can achieve symmetric or asymmetric suppressions or amplifications of double OMIT peaks, which is accompanied by either significantly enhanced advance or a transition from advance to delay of the signal light. Our results confirm that multi-mode OMIT devices with selective acoustic control, provide a versatile route to realize coherent multi-band modulations, switchable signal amplifications, and COM based light communications.

II. THEORETICAL MODEL

We consider a three-mode COM system composed of an optical resonator with two MRs (see Fig. 1). The MR₁ couples not only with the cavity field (via radiation pressure force), but also with the MR₂ (through the position-position coupling). As shown in experiments, the position-position coupling can be realized by e.g., us-

* jinghui73@gmail.com

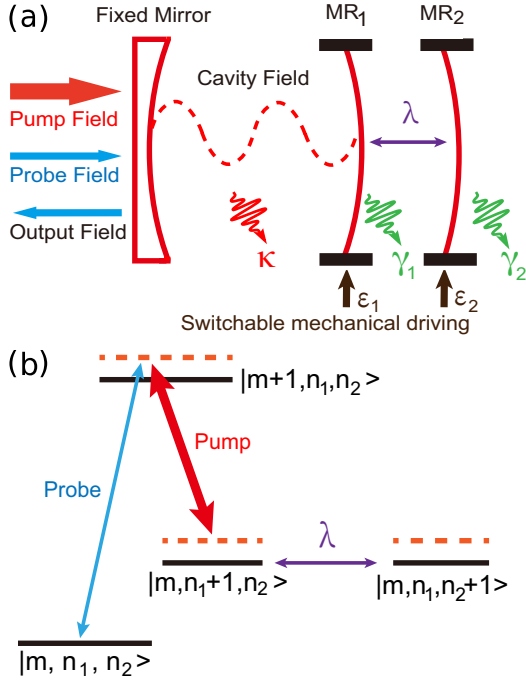


FIG. 1. (Color online) (a) Schematic illustration of the compound COM system. The cavity is driven by a pump field at frequency ω_l and a weak probe field at frequency ω_p , with the optical amplitudes ε_l , ε_p , and the phases ϕ_l , ϕ_p , respectively. The selective mechanical driving of MRs provides extra control of OMIT, with amplitude ε_1 (ε_2) at frequency ω_1 (ω_2). κ and γ_i ($i = 1, 2$) are the optical and mechanical decay rates, respectively. (b) Energy-level structures of this system, where $|m\rangle$, $|n_1\rangle$ and $|n_2\rangle$ denote the number states of the cavity mode and the mechanical modes, respectively.

ing a piezoelectric transducer[57], or applying an electrostatic force between the MRs [85, 86]. For two MRs coupled by the Coulomb force [85–87], the interaction between them is written in the simple level as

$$H_{\text{coul}} = \frac{-k_e q_1 q_2}{|r_0 + x_1 - x_2|}, \quad (1)$$

where k_e is the electrostatic constant, r_0 is the equilibrium separation of the two charged oscillators in absence of any interaction between them, and m_i ($i = 1, 2$) or $q_i = C_i V_i$ is the effective mass or the charge of the MR $_i$, with C_i and V_i being the capacitance and the voltage of the bias gate, respectively. x_i ($i = 1, 2$) is the small oscillations of the MR $_i$ from their equilibrium position. In the case of $r_0 \gg \{x_1, x_2\}$, with the second-order expansion, one can expand

$$H_{\text{coul}} \simeq \frac{-k_e q_1 q_2}{r_0} \left[1 - \frac{x_1 - x_2}{r_0} + \left(\frac{x_1 - x_2}{r_0} \right)^2 \right], \quad (2)$$

here the constant term and the linear term which can be absorbed into the definition of the equilibrium positions, and the quadratic term includes a renormaliza-

tion of the oscillation frequency for the two MRs. Moreover, the small oscillations of the two mechanical oscillators from their equilibrium positions can be represented $x_i = \sqrt{\hbar/2m_i\omega_{m,i}}(b_i + b_i^\dagger)$ ($i = 1, 2$). Therefore, the effective Coulomb interaction can be simplified as

$$\mathcal{H}_{\text{coul}} = -\frac{2k_e C_1 V_1 C_2 V_2}{r_0^3} x_1 x_2 = \hbar \lambda (b_1^\dagger b_2 + b_1 b_2^\dagger), \quad (3)$$

here λ is the Coulomb interaction strength

$$\lambda = \frac{k_e C_1 V_1 C_2 V_2}{r_0^3} \sqrt{\frac{\hbar}{m_1 m_2 \omega_{m,1} \omega_{m,2}}}, \quad (4)$$

for the typical experimental parameters $r_0 = 2$ mm, $C_1 = C_2 = 27.5$ nF, and $V_1 = V_2 = 1$ V [85, 86], we find $\lambda \simeq 0.1$ MHz. Table I shows more relevant parameters of experimentally achieved coupled MRs. The cavity is driven by a pump field and a weak probe field. Meanwhile, as also shown in experiments [27, 88, 89], mechanical driving fields with frequency ω_i and phase ϕ_i ($i = 1, 2$) can be applied to selectively pump the MRs. We note that in the simplest two-mode COM (i.e., without the MR $_2$), pumping the MR $_1$ leads to a closed-loop Δ -type energy-level structure [see Fig. 1(b)], under which optical properties of the system become highly sensitive to the mechanical pump parameters [78–83]. In the presence of coupled two MRs, as shown in a recent experiment [27], the effective phonon-phonon coupling also can be enhanced by the mechanical pump. Inspired by these works, here we show that by selectively driving the MRs, significantly different OMIT properties can be revealed, which offers flexible ways to control light in practice.

In the rotating frame at the pump frequency, the total Hamiltonian of the system can be written at the simplest level as

$$\begin{aligned} H &= H_0 + H_{\text{int}} + H_{\text{dr}}, \\ H_0 &= \hbar \Delta_c c^\dagger c + \hbar \omega_{m,1} b_1^\dagger b_1 + \hbar \omega_{m,2} b_2^\dagger b_2, \\ H_{\text{int}} &= -\hbar g c^\dagger c (b_1^\dagger + b_1) + \hbar \lambda (b_1^\dagger b_2 + b_1 b_2^\dagger), \\ H_{\text{dr}} &= i\hbar \sum_{j=1,2} \varepsilon_j b_j^\dagger e^{-i\omega_j t - i\phi_j} + i\hbar \varepsilon_l c^\dagger \\ &\quad + i\hbar \varepsilon_p c^\dagger e^{-i\xi t - i\phi_{pl}} - \text{H.c.}, \end{aligned} \quad (5)$$

where c or b_i ($i = 1, 2$) is the annihilation operator of the cavity field with frequency ω_c or the MR $_i$ with frequency $\omega_{m,i}$, respectively. $\Delta_c = \omega_c - \omega_l$, $\phi_{pl} = \phi_p - \phi_l$, and g denotes the optomechanical coupling coefficient. In the following, we focus on the features of OMIT by selectively driving the MRs, including the signal transmission, group delay, and its higher-order sidebands.

For this purpose, the equations of motion (EOM) of this system are

$$\begin{aligned} \dot{c} &= -\left(i\Delta_c + \frac{\kappa}{2}\right) c + ig(b_1^\dagger + b_1)c + \varepsilon_l + \varepsilon_p e^{-i\xi t - i\phi_{pl}}, \\ \dot{b}_1 &= -\left(i\omega_{m,1} + \frac{\gamma_1}{2}\right) b_1 + igc^\dagger c - i\lambda b_2 + \varepsilon_1 e^{-i\xi t - i\phi_1}, \\ \dot{b}_2 &= -\left(i\omega_{m,2} + \frac{\gamma_2}{2}\right) b_2 - i\lambda b_1 + \varepsilon_2 e^{-i\xi t - i\phi_2}, \end{aligned} \quad (6)$$

TABLE I. Experimental parameters of the mechanical resonators

Reference	Material	Mechanical frequency $\omega_1(\omega_2)$	Damping rate $\gamma_1(\gamma_2)$	Coupling form
L. Fan <i>et al.</i> [27]	AlN	6.87 GHz (456.5 MHz)	105.5 kHz (8.478 kHz)	nonlinearly
Q. Lin <i>et al.</i> [56]	Si ₃ N ₄ / SiO ₂	8.3 MHz (13.6 MHz)	2.1 MHz (0.11 MHz)	linearly
H. Okamoto <i>et al.</i> [57]	GaAs	1.845 MHz (1.848 MHz)	131.9 Hz (131.9 Hz)	linearly
M. J. Weaver <i>et al.</i> [58]	Si ₃ N ₄	297 kHz (659 kHz)	9.42 Hz (6.28 Hz)	linearly

κ and γ_i ($i = 1, 2$) are the optical and mechanical decay rates, respectively. In the case of $\{\varepsilon_p, \varepsilon_i\} \ll \varepsilon_l$, we express the dynamical variables as the sum of their steady-state values and small fluctuations, i.e., $c = c_s + \delta c$ and $b = b_{i,s} + \delta b_i$ ($i = 1, 2$). The steady-state values of the dynamical variables are

$$\begin{aligned} c_s &= \frac{\varepsilon_l}{i\Delta + \frac{\kappa}{2}}, \\ b_{1,s} &= \frac{ig|c_s|^2 - i\lambda b_{2,s}}{i\omega_{m,1} + \frac{\gamma_1}{2}}, \\ b_{2,s} &= \frac{-i\lambda b_{1,s}}{i\omega_{m,2} + \frac{\gamma_2}{2}}, \end{aligned} \quad (7)$$

here $\Delta = \Delta_c - g(b_{1,s}^* + b_{1,s})$. To calculate the amplitudes of the first-order and second-order sidebands, we assume that the fluctuation terms δa and δb_i ($i = 1, 2$) have the following forms [36]

$$\begin{aligned} \delta c &= A_1^- e^{-i\xi t} + A_1^+ e^{i\xi t} + A_2^- e^{-2i\xi t} + A_2^+ e^{2i\xi t}, \\ \delta b_1 &= B_1^- e^{-i\xi t} + B_1^+ e^{i\xi t} + B_2^- e^{-2i\xi t} + B_2^+ e^{2i\xi t}, \\ \delta b_2 &= D_1^- e^{-i\xi t} + D_1^+ e^{i\xi t} + D_2^- e^{-2i\xi t} + D_2^+ e^{2i\xi t}. \end{aligned} \quad (8)$$

Substituting Eq. (8) into Eq. (6) leads to twelve equations. We can simplify these twelve equations into two groups [36]: one group describes the process of the first-

order sideband which corresponds to the linear case

$$\begin{aligned} h_1^+ A_1^- &= iG(B_1^{+*} + B_1^-) + \varepsilon_p e^{-i\phi_{pl}}, \\ h_1^- A_1^{+*} &= -iG^*(B_1^- + B_1^{+*}), \\ h_2^+ B_1^- &= iGA_1^{+*} + iG^* A_1^- - i\lambda D_1^- + \varepsilon_1 e^{-i\phi_1}, \\ h_2^- B_1^{+*} &= -iG^* A_1^- - iGA_1^{+*} + i\lambda D_1^{+*}, \\ h_3^+ D_1^- &= -i\lambda B_1^- + \varepsilon_2 e^{-i\phi_2}, \\ h_3^- D_1^{+*} &= i\lambda B_1^{+*}, \end{aligned} \quad (9)$$

and the other group describes the the second-order sideband

$$\begin{aligned} h_4^+ A_2^- &= iG(B_2^{+*} + B_2^-) + ig(A_1^- B_{1+}^* + A_1^- B_{1-}), \\ h_4^- A_2^{+*} &= -iG^*(B_2^{+*} + B_2^-) - ig(A_1^{+*} B_1^- + A_1^{+*} B_1^{+*}), \\ h_5^+ B_2^- &= iGA_2^{+*} + iG^* A_2^- + igA_1^- A_1^{+*} - i\lambda D_2^-, \\ h_5^- B_2^{+*} &= -iG^* A_2^- - iGA_2^{+*} - igA_1^- A_1^{+*} + i\lambda D_2^{+*}, \\ h_6^+ D_2^- &= -i\lambda B_2^-, \\ h_6^- D_2^{+*} &= i\lambda B_2^{+*}, \end{aligned} \quad (10)$$

here $G = gc_s$ and

$$\begin{aligned} h_1^\pm &= \pm i\Delta + \frac{\kappa}{2} - i\xi, & h_2^\pm &= \pm i\omega_{m,1} + \frac{\gamma_1}{2} - i\xi, \\ h_3^\pm &= \pm i\omega_{m,2} + \frac{\gamma_2}{2} - i\xi, & h_4^\pm &= \pm i\Delta + \frac{\kappa}{2} - 2i\xi, \\ h_5^\pm &= \pm i\omega_{m,1} + \frac{\gamma_1}{2} - 2i\xi, & h_6^\pm &= \pm i\omega_{m,2} + \frac{\gamma_2}{2} - 2i\xi. \end{aligned}$$

By solving Eq. (9) and Eq. (10) leads to

$$A_1^- = \left[\frac{(h_1^- U_1^+ U_1^- + |G|^2 \Pi) \varepsilon_p}{h_1^+ h_1^- U_1^+ U_1^- + 2i\Delta |G|^2 \Pi} + \frac{iG h_1^- h_3^+ U_1^- \varepsilon_1 e^{-i\Phi_1}}{h_1^+ h_1^- U_1^+ U_1^- + 2i\Delta |G|^2 \Pi} + \frac{G h_1^- U_1^- \lambda \varepsilon_2 e^{-i\Phi_2}}{h_1^+ h_1^- U_1^+ U_1^- + 2i\Delta |G|^2 \Pi} \right] e^{-i\phi_{pl}}, \quad (11)$$

and

$$A_2^- = \frac{-i\xi g G \Gamma - g h_4^- U_2^+ U_2^- (h_1^- / G^*)}{h_4^+ h_4^- U_2^+ U_2^- + 2i\Delta |G|^2 \Gamma} A_1^- A_1^{+*} + \frac{g G^2 \Gamma (h_1^- / G^*)}{h_4^+ h_4^- U_2^+ U_2^- + 2i\Delta |G|^2 \Gamma} (A_1^{+*})^2, \quad (12)$$

here

$$\begin{aligned} \Phi_i &= \phi_i - \phi_{pl} = \phi_i + \phi_l - \phi_p, \\ U_1^\pm &= h_2^\pm h_3^\pm + \lambda^2, & \Pi &= h_3^- U_1^+ - h_3^+ U_1^-, \\ U_2^\pm &= h_5^\pm h_6^\pm + \lambda^2, & \Gamma &= U_2^+ h_6^- - U_2^- h_6^+. \end{aligned}$$

With these at hand, by using the input-output relation [90]

$$c^{\text{out}} = c^{\text{in}} - \sqrt{\eta_c \kappa} A_1^-,$$

where c^{in} and c^{out} are the input and output field operators, respectively, we can obtain the transmission rate of

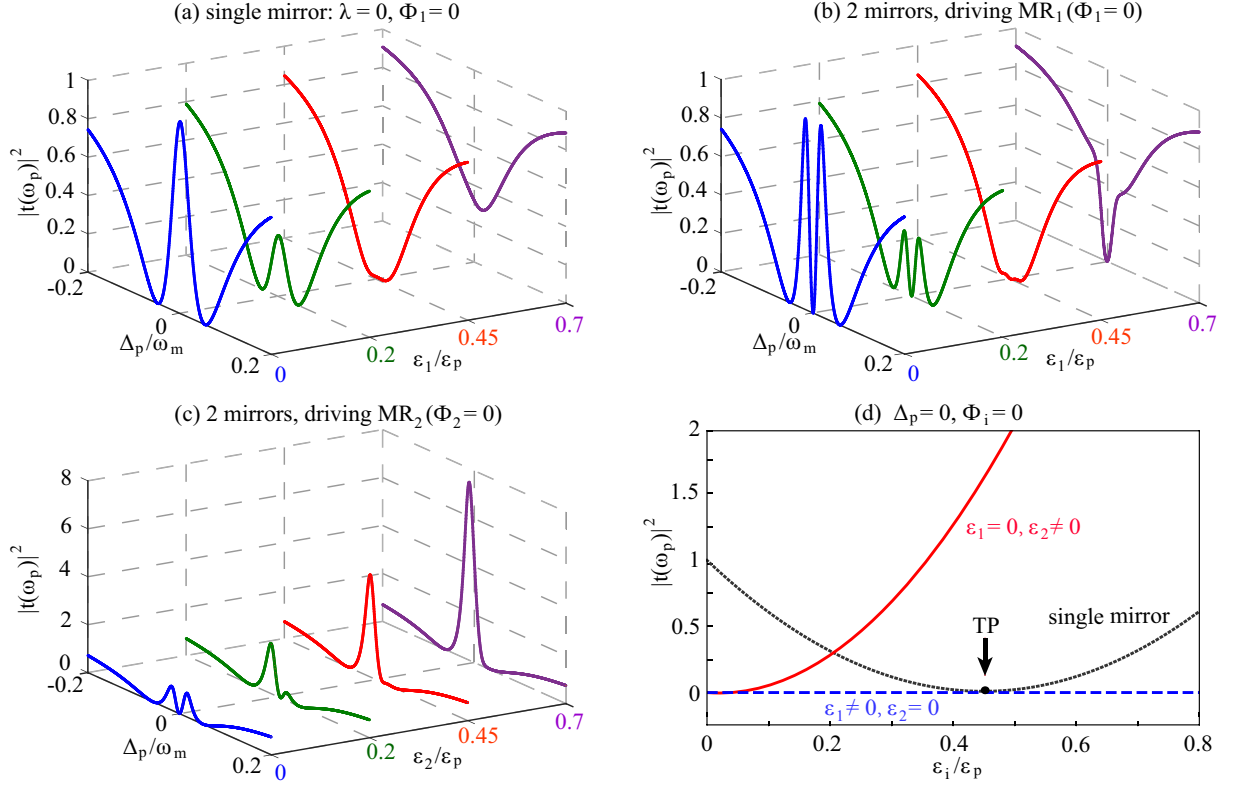


FIG. 2. (Color online) (a-c) Transmission of the probe light as a function of the optical detuning Δ_p/ω_m with different values of the amplitude ε_i ($i = 1, 2$). (d) For $\Delta_p = 0$, transmission of the probe light as a function of the amplitude ε_i ($i = 1, 2$).

the probe as

$$|t(\omega_p)|^2 = \left| 1 - \frac{\eta_c \kappa A_1^-}{\varepsilon_p e^{-i\phi_{pl}}} \right|^2. \quad (13)$$

In Eq. (11), the first term is the contribution from the standard OMIT process due to the destructive interference of the probe absorption [19, 20]. The second and third term are the contribution from the phonon-photon parametric process [78] and the phonon-phonon parametric process [27], induced by driving the MR_1 and MR_2 . Clearly, these parametric process can modify and control the transmission of the signal field by adjusting the amplitude ε_i and the photon-phonon mixing phase Φ_i ($i = 1, 2$).

III. RESULTS AND DISCUSSION

A. Linear OMIT spectrum

In our numerical simulations, to demonstrate that the observation of the signal transmission is within current experimental reach, we calculate Eq. (13) and (17) with parameters from Ref. [42, 58, 85–87]: $\omega_{m,i}/2\pi = 947$ kHz ($i = 1, 2$), $m_i = 145$ ng, $\gamma_i = \omega_{m,i}/Q$, $\kappa/2\pi = 215$ kHz, $Q = 6700$, $\lambda_l = 1064$ nm, $L = 25$ mm, $\lambda = 0.1$ MHz, and

$P_L = 3$ mW. We have confirmed that for the pump power $P_L < 7$ mW, single stable solution exists and the compound system has no bistability (see stability analysis in Appendix A).

Figure 2 shows the transmission rate $|t(\omega_p)|^2$ as a function of the optical detuning $\Delta_p/\omega_m = (\xi - \omega_m)/\omega_m$ and the phase Φ_1 . For comparisons, we first consider the single-mirror case ($\lambda = 0$). As in standard COM system (without any mechanical driving), a standard single transparency window emerges around the resonance point $\Delta_p = 0$ [see the blue solid line in Fig. 2(a)], as a result of the destructive interference of two absorption channels of the probe photons (by the cavity or by the phonon mode) [19, 20]. When a mechanical driving field is applied to the MR_1 , there are three coupling pathways of this system. The transitions $|m, n_1, n_2\rangle \leftrightarrow |m+1, n_1, n_2\rangle$, $|m, n_1+1, n_2\rangle \leftrightarrow |m+1, n_1, n_2\rangle$, and $|m, n_1, n_2\rangle \leftrightarrow |m, n_1+1, n_2\rangle$ can be achieved by applying a probe field, an optical pump field, and a mechanical pump field. Clearly, the three couplings result in a closed-loop Δ -type transition structure, leading to the phase-sensitive optical behaviors of the OMIT system [78–80]. As shown in Fig. 2(a), the transmission rate at $\Delta_p = 0$ can be firstly suppressed and then amplified by increasing the mechanical driving strength due to the interference between the OMIT process and the phonon-photon parametric process [represented by the first and the second

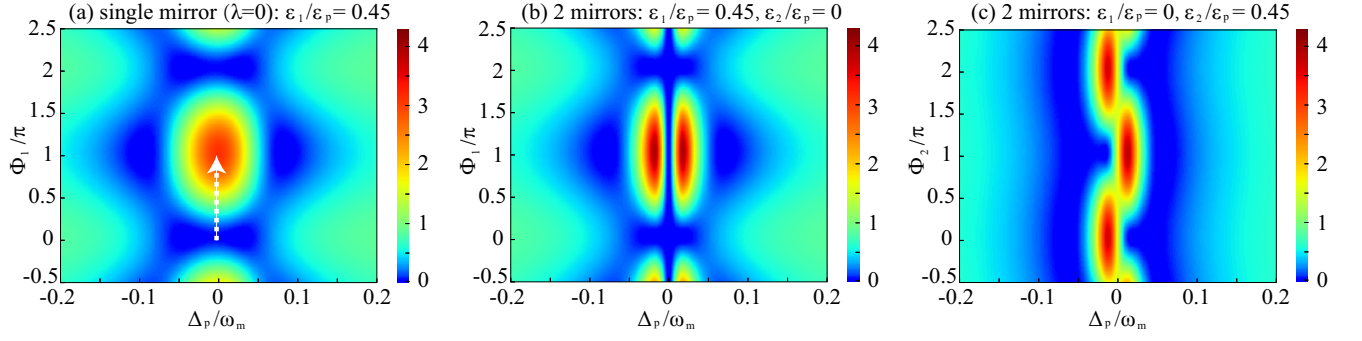


FIG. 3. (Color online) (a) For single mirror ($\lambda = 0$), the transmission as a function of the optical detuning Δ_p/ω_m and the phase Φ_1 . (b,c) For two mirrors, transmission of the probe light as a function of the optical detuning Δ_p/ω_m and the phase Φ_i ($i = 1, 2$).

terms in Eq. (11), respectively]. By setting $|t(\omega_p)|^2 = 0$, the turning point (TP) position turns out to be

$$\left(\frac{\epsilon_1}{\epsilon_p}\right)_{\text{TP}} = \frac{\omega_{m,1}\kappa + \Delta\gamma_1 - \omega_{m,1}\eta\kappa\alpha}{2Gh_1^+h_1^-h_2^+h_2^-\eta\kappa}, \quad (14)$$

with

$$\alpha = 2h_1^+h_1^-h_2^+h_2^- + |G|^2\kappa\gamma_1 - 4\Delta\omega_{m,1}|G|^2, \quad (15)$$

which, for the parameter values chosen here, corresponds to $(\epsilon_1/\epsilon_p)_{\text{TP}} \simeq 0.45$.

For $\lambda \neq 0$, in the absence of any mechanical driving, double OMIT spectrum is known to appear in the two-mirror system [see the blue solid line in Fig. 2(b)], i.e., the purely mechanical coupling splits the original single-mirror OMIT peak into two [44, 87]. Now we study the new features of double OMIT with switchable mechanical driving applied to either MR₁ or MR₂.

By driving the MR₁, both effective optomechanical coupling and phonon-phonon coupling can be enhanced [27] and a closed-loop Δ -type energy-level transitions configuration is formed in this system (for similar systems, see Refs. [78–80]). This leads to symmetric suppressions ($\Phi_1 = 0$) or amplifications ($\Phi_1 = \pi$) for both OMIT peaks [see Fig. 2(b)], with a resonant absorption dip at $\Delta_p = 0$ [Fig. 2(b) and the blue dashed line in Fig. 2(d)]. In contrast, by driving the MR₂, with the enhanced phonon-phonon coupling [27], highly asymmetric Fano-like OMIT spectrum appears due to the competition between the OMIT process and the phonon-phonon coupling process, corresponding to the first and the third terms in Eq. (11), respectively, as shown in Fig. 2(c). The physics of these features can be explained as follows: In such a system, the MR₁ couples not only with the cavity field, but also with the MR₂. By driving the MR₁, both effective optomechanical coupling and phonon-phonon coupling can be enhanced (see e.g., Ref. [27] for similar results). However, by driving the MR₂, only effective phonon-phonon coupling can be enhanced. Thus, as expected, asymmetric amplifications of the signal light can be achieved by selectively driving the MR₂. These in-

tuitive pictures agree well with our numerical results as shown in Fig. 2.

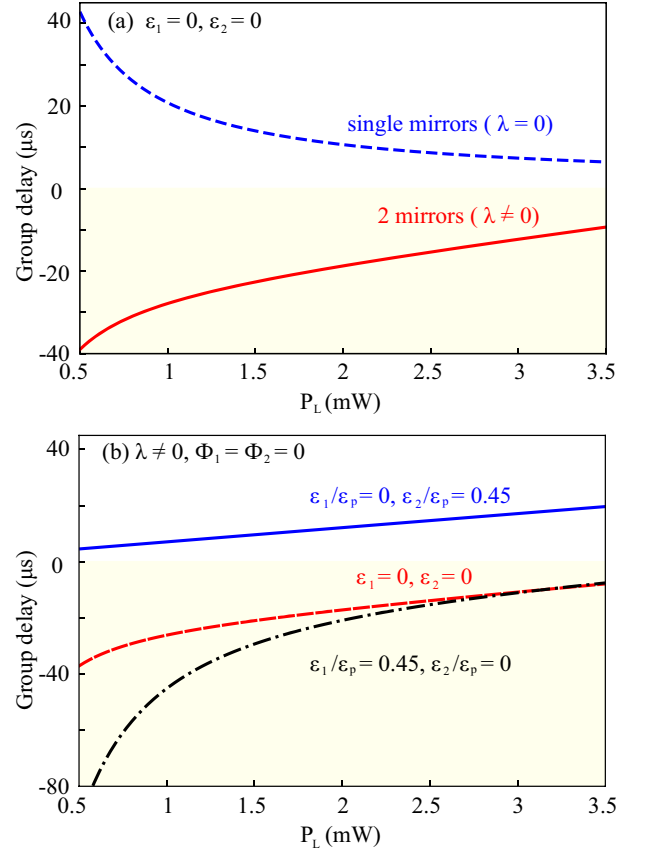


FIG. 4. (Color online) (a, b) For $\Delta_p = 0$, group delay of the probe light τ_g (in the unit of μs) as a function of the pump power P_L .

Interestingly, for single mirror case, the transmission of the probe light changes periodically with the phase Φ_1 [see Fig. 3(a)]. For example, with $\epsilon_1/\epsilon_p = 0.45$, the transmission rate changes from strong absorption to amplification by tuning the phase Φ_1 from 0 to π . Also, for two mirrors case, periodic changes of the optical transmission

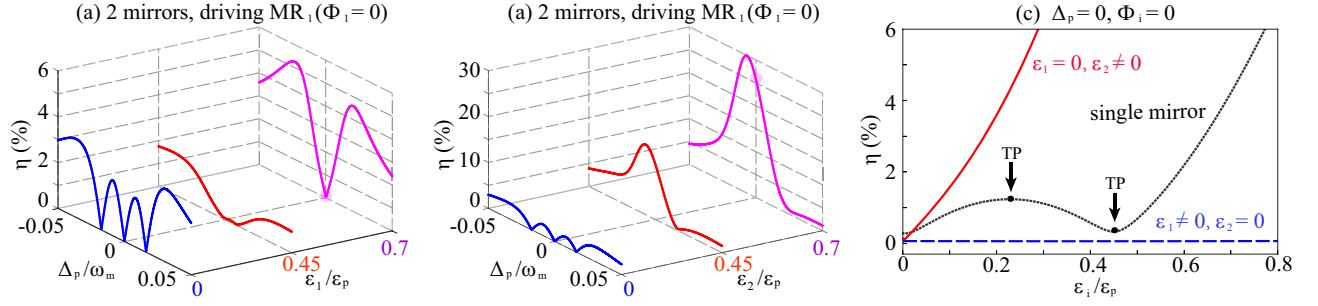


FIG. 5. (Color online) The efficiency of second-order sideband as a function of the optical detuning Δ_p/ω_m with different values of the amplitude (a) $\varepsilon_1/\varepsilon_p$ and (b) $\varepsilon_2/\varepsilon_p$. (c) For $\Delta_p = 0$, the efficiency of second-order sideband as a function of the amplitude $\varepsilon_i/\varepsilon_p$ ($i = 1, 2$).

rate can be found by varying the phase of the mechanical driving field [see Fig. 3(b) and Fig. 3(c)]. Hence, more flexible OMIT control of the signal light becomes accessible by selective driving the MRs, e.g., the signal can be completely blocked or greatly amplified by driving the MR₁ or MR₂, at the resonance point $\Delta_p = 0$. This ability of selectively switching and amplifying the input weak signal could be highly desirable in practical optical communications [78–81, 91].

B. Optical group delay

The group delay of the transmitted light is given by

$$\tau_g = \frac{d \arg[t(\omega_p)]}{d\omega_p} \Big|_{\omega_p=\omega_c}. \quad (16)$$

Accompanying with the standard single-mirror OMIT, slow light [see the blue dashed line in Fig. 4(a)] can emerge due to the abnormal dispersion [23]. In contrast, by introducing active gain into the system, fast light can be observed in experiments [32, 79, 92]. A merit of our system is the ability to selectively achieve either slow light or fast light by controlling the mechanical parameters. Figure 4(b) shows that by driving the MR₁, significant enhancement of the light advance can be observed in comparison with the case without any mechanical pump [see the blue dashed line in Fig. 4(b)]. However, by driving the MR₂, a tunable switch from fast to slow light can be achieved [see the blue solid line in Fig. 4(b)]. For $P_L = 3.5$ mW, in comparison with the single-mirror system, ~ 5 times enhancement can be observed for the group delay by using the two-mirror device. This is useful for achieving a multi-functional amplifier with the extra ability to selectively tune the optical group velocities.

C. Nonlinear higher-order sidebands

As defined in Ref. [36], the efficiency of the second-order sideband process is

$$\eta = \left| -\frac{\eta_c \kappa A_2^-}{\varepsilon_p e^{-i\phi_{pl}}} \right|. \quad (17)$$

Due to nonlinear optomechanical interactions, in the OMIT process, output fields with frequencies $\omega_l \pm n\xi$ can emerge, where n is an integer representing the order of the sidebands [36]. The output fields with frequencies $\omega_l + 2\xi$ is the second order upper sideband, while $\omega_l - 2\xi$ is the lower sideband. In this work, we only consider the second-order upper sideband. For the single-mirror case, in the absence of any mechanical driving, the second-order sideband is subdued when the OMIT occurs, which results in a local minimum between the two sideband peaks around $\Delta_p = 0$ [36]. The efficiency of second-order sideband η is, however, extremely small in conventional COM systems, e.g., 1%–3% [36].

As shown in Fig. 5, by driving the MR₁, i.e., η remains almost unchanged at the resonance [see Fig. 5(a) and the blue dashed line in Fig. 5(c)], which is similar to the linear OMIT spectrum [see the blue dashed line in Fig. 2(d)]. In contrast, by driving the MR₂, giant enhancement of the second-order sideband can be observed at the resonance [see the red solid line in Fig. 5(c)]. For example, for $\varepsilon_2/\varepsilon_p = 0.7$, the efficiency η is about 25% [see the purple solid line in Fig. 5(b)], which is in sharp contrast to the corresponding result $\eta \approx 0$ by driving MR₁. This giant enhancement of second-order sidebands, with much narrower bandwidth, can be used in precision measurement of very weak signals, e.g., single-charge detections [45, 46].

IV. CONCLUSION

In conclusion, we have studied the mechanically controlled optical amplification and tunable group delay in a compound system composed of an optical resonator and

two coupled mechanical resonators. We find that by driving one of the mechanical modes, both OMIT peaks can be symmetrically suppressed or amplified, which is accompanied by significantly enhanced light advance. In contrast, by driving the other mechanical mode, the OMIT spectrum becomes highly asymmetric, accompanied by a transition from fast light to slow light. In addition, periodic changes of both the linear OMIT spectrum and the higher-order sidebands can be observed by tuning the phases of the mechanical driving fields. These features of selective OMIT amplifications and switchable group delays of light provide more flexible ways in practical applications ranging from optical storage or modulations to multi-band optical communications. In future works, it will be also of interests to study the role of selective mechanical driving in enhancing or steering, for examples, light-sound entanglement [93, 94], photon-phonon mutual blockade [95], precision measurement [45, 46], and switchable amplification of light or sound.

Note added. After completing this work, we became aware of a preprint also on OMIT utilizing an acoustic dimer, but with only a fixed mechanical pump [96].

V. ACKNOWLEDGMENTS

This work is supported by the National Natural Science Foundation of China (NSFC) under Grants No. 11474087 and No. 11774086, and the HuNU Program for Talented Youth.

Appendix A: Stability analysis

Considering photon damping and the Brownian noise from the cavity and the environment, the EOM are given by

$$\begin{aligned}\dot{c} &= -\left(i\Delta_c + \frac{\kappa}{2}\right)c + ig(b_{1,s}^\dagger + b_{1,s})c + \varepsilon_l + \sqrt{2\kappa}c_{\text{in}}(t), \\ \dot{b}_1 &= -\left(i\omega_{m,1} + \frac{\gamma_1}{2}\right)b_1 + igc^\dagger c - i\lambda b_2 + \sqrt{2\gamma_1}\xi_1(t), \\ \dot{b}_2 &= -\left(i\omega_{m,2} + \frac{\gamma_2}{2}\right)b_2 - i\lambda b_1 + \sqrt{2\gamma_2}\xi_2(t),\end{aligned}\quad (\text{A1})$$

where $c_{\text{in}}(t)$ is the input noise operator with zero mean value, and $\xi_i(t)$ ($i = 1, 2$) is the Brownian noise operators associated with the damping of the MR_i . Under the Markov approximation, two-time correlation functions of these input noise operators are

$$\begin{aligned}\langle \hat{c}_{\text{in}}(t) \hat{c}_{\text{in}}(t') \rangle &= \delta(t - t'), \\ \langle \xi_i(t) \xi_i(t') \rangle &= (n_{\text{th}} + 1) \delta(t - t') \quad (i = 1, 2),\end{aligned}\quad (\text{A2})$$

here $n_{\text{th}} = (e^{\hbar\omega/k_B T} - 1)^{-1}$, with k_B is the Boltzmann constant and T is the bath temperature. By setting all the time derivatives to zero of Eq. (A1), the steady-state

value of c is

$$c_s = \frac{\varepsilon_l}{(i\Delta + \frac{\kappa}{2})}, \quad (\text{A3})$$

where $\Delta = \Delta_c - g(b_{1,s}^\dagger + b_{1,s})$ is the effective detuning, including the effects of radiation pressure and Coulomb interaction. We now study the steady-state behavior of the mean photon number $|c_s|^2$. In this case, using Eq. (A3), it is straightforward to show that $|c_s|^2$ satisfies

$$|c_s|^2 \left(\Delta^2 + \frac{\kappa^2}{4} \right) = |\varepsilon_l|^2. \quad (\text{A4})$$

We provide a direct and efficient estimation on how many positive solutions exist in Eq. (A4) according to the Descartes rule. Eq. (A4) can be recast as

$$a_3 x^3 + a_2 x^2 + a_1 x + a_0 = 0, \quad (\text{A5})$$

where we define $x = |c_s|^2$, and the coefficients are

$$\begin{aligned}a_3 &= W^2 g^4, & a_2 &= -2\Delta_c W g^2, \\ a_1 &= \frac{\kappa^2}{4} + \Delta_c^2, & a_0 &= -\varepsilon_l^2,\end{aligned}\quad (\text{A6})$$

with

$$W = \frac{2\omega_{m,1} \left(\omega_{m,2}^2 + \frac{\gamma_2^2}{4} \right) - 2\lambda^2 \omega_{m,2}}{\left(\omega_{m,1}^2 + \frac{\gamma_1^2}{4} \right)^2 - 2\lambda^2 \left(\omega_{m,2} \omega_{m,1} - \frac{\gamma_1 \gamma_2}{4} \right) + \lambda^4}, \quad (\text{A7})$$

here all parameters $g, \kappa, \lambda, \omega_{m,1}, \omega_{m,2}, \gamma_1, \gamma_2$, and ε_l in Eq. (A6) are positive, we have $a_0 < 0, a_1 > 0, a_2 < 0$ and $a_3 > 0$, corresponding to the following unique sign sequence:

$$\text{sgn}(a_3), \dots, \text{sgn}(a_0) = + - + -. \quad (\text{A8})$$

According to the Descartes rule, Eq. (A5) has three real

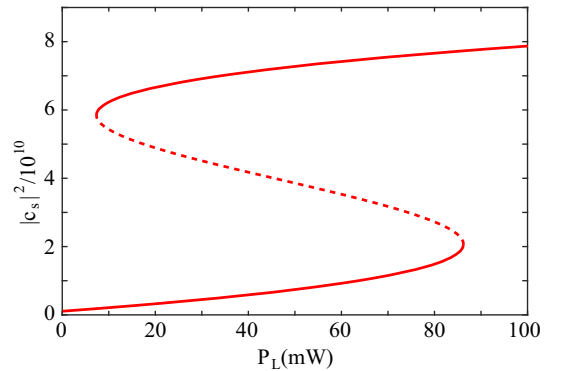


FIG. 6. (Color online) Mean intracavity photon number $|c_s|^2$ as a function of the pump power P_L with $\lambda = 0.1$ MHz.

solutions at most, two of which are dynamically stable.

We also have checked numerically that the parameters we chosen in this paper satisfy the stability condition. When the cavity is driven on its red sideband, Figure 6 shows the mean intracavity photon number $|c_s|^2$ as a function of pump power P_L with $\lambda = 0.1$ MHz. It can be seen that the mean photon number exhibits the standard S-shaped bistability. As the pump power P_L increases from zero, there is only single stable solution of Eq. (A5) at the beginning. However, when P_L is larger than a critical value, there are three real solutions. The largest and smallest solutions are stable, and the middle one is unstable.

Below we determine the stability of the steady states of our system using the Routh-Hurwitz criterion [97]. The fluctuation terms of the EOM are

$$\begin{aligned}\delta\dot{c} &= -\left(i\Delta + \frac{\kappa}{2}\right)\delta c + iG(\delta b_1^\dagger + \delta b_1) + \sqrt{2\kappa}\delta\hat{c}_{in}(t), \\ \delta\dot{b}_1 &= -\left(i\omega_{m,1} + \frac{\gamma_1}{2}\right)\delta b_1 + iG\delta c^\dagger + iG^*\delta c - i\lambda\delta b_2 \\ &\quad + \sqrt{2\gamma_1}\delta\xi_1(t), \\ \delta\dot{b}_2 &= -\left(i\omega_{m,2} + \frac{\gamma_2}{2}\right)\delta b_2 - i\lambda\delta b_1 + \sqrt{2\gamma_2}\delta\xi_2(t),\end{aligned}\quad (\text{A9})$$

here $G = gc_s$. In a compact matrix form, Eq. (A9) can

be recast as

$$\delta\dot{\mathbf{u}} = \mathbf{C}\mathbf{u} + \delta\mathbf{v}_{in}, \quad (\text{A10})$$

where vectors $\mathbf{u} = (\delta c, \delta c^\dagger, \delta b_1, \delta b_1^\dagger, \delta b_2, \delta b_2^\dagger)^T$ and $\delta\mathbf{v}_{in} = \sqrt{2}(\sqrt{\kappa}\delta\hat{c}_{in}, \sqrt{\kappa}\delta\hat{c}_{in}^\dagger, \sqrt{\gamma_1}\delta\xi_1, \sqrt{\gamma_1}\delta\xi_1^\dagger, \sqrt{\gamma_2}\delta\xi_2, \sqrt{\gamma_2}\delta\xi_2^\dagger)^T$, in which T denotes the transpose of a matrix. The matrix \mathbf{C} is given by

$$\mathbf{C} = \begin{pmatrix} -i\Delta - \frac{\kappa}{2} & 0 & iG & iG & 0 & 0 \\ 0 & i\Delta - \frac{\kappa}{2} & iG^* & iG^* & 0 & 0 \\ -i\omega_{m,1} - \frac{\gamma_1}{2} & 0 & iG^* & iG & -i\lambda & 0 \\ 0 & i\omega_{m,1} - \frac{\gamma_1}{2} & iG & iG^* & 0 & i\lambda \\ -i\omega_{m,2} - \frac{\gamma_2}{2} & 0 & -i\lambda & 0 & 0 & 0 \\ 0 & i\omega_{m,2} - \frac{\gamma_2}{2} & 0 & i\lambda & 0 & 0 \end{pmatrix}.$$

The characteristic equation $|\mathbf{C} - \Upsilon\mathbf{I}| = 0$ can be reduced to $\Upsilon^6 + C_1\Upsilon^5 + C_2\Upsilon^4 + C_3\Upsilon^3 + C_4\Upsilon^2 + C_5\Upsilon + C_6 = 0$, where the coefficients can be derived using straightforward but tedious algebra. From the Routh-Hurwitz criterion [97], a solution is stable only if the real part of the corresponding eigenvalue Υ is negative and the stability conditions can then be obtained as

$$\begin{aligned}C_1 &> 0, \\ C_1C_2 - C_3 &> 0, \\ C_1C_2C_3 + C_1C_5 - C_1^2C_4 - C_3^2 &> 0, \\ C_1C_2C_3C_4 + C_2C_6(C_1^2 + C_3) + C_1C_5(C_4 + C_5) - C_1^2C_4^2 - C_1C_3C_6 - C_3^2C_4 - C_4^2 &> 0, \\ C_1C_2C_3C_4C_5 + (C_1^2C_2 - C_2C_3 + C_1C_3)C_5C_6 + (C_3C_2 + C_1C_4 - C_1C_2^2 - C_5)C_5^2 - (C_1C_2C_6 + C_4C_5)C_3^2 &> 0, \\ C_1C_2C_3C_4C_5C_6 + (C_1C_4^2 - C_1^2C_4^2 - C_3^2C_4)C_5C_6 + C_2C_3C_5^2C_6 - C_1C_2C_3^2C_6^2 - C_1C_3C_5C_6^2 - C_5^3C_6 &> 0.\end{aligned}\quad (\text{A11})$$

Through these analyses, we have confirmed that the experimentally accessible parameters in the main

manuscript can keep the compound system in a stable zone.

-
- [1] M. Aspelmeyer, T. J. Kippenberg, and F. Marquardt, Cavity optomechanics, *Rev. Mod. Phys.* **86**, 1391 (2014).
 - [2] M. Metcalfe, Applications of cavity optomechanics, *App. Phys. Rev.* **1**, 031105 (2014).
 - [3] T. Bagci, A. Simonsen, S. Schmid, L. G. Villanueva, E. Zeuthen, J. Appel, J. M. Taylor, A. S. Sorensen, K. Usami, A. Schliesser, and E. S. Polzik, Optical detection of radio waves through a nanomechanical transducer, *Nature (London)* **507**, 81 (2014).
 - [4] F. Lecocq, J. B. Clark, R. W. Simmonds, J. Aumentado, and J. D. Teufel, Mechanically Mediated Microwave Frequency Conversion in the Quantum Regime, *Phys. Rev. Lett.* **116**, 043601 (2016).
 - [5] C. F. Ockeloen-Korppi, E. Damskagg, J.-M. Pirkkalainen, T. T. Heikkilä, F. Massel, and M. A.

-
- Sillanpää, Low-Noise Amplification and Frequency Conversion with a Multiport Microwave Optomechanical Device, *Phys. Rev. X* **6**, 041024 (2016).
 - [6] E. Gavartin, P. Verlot, and T. J. Kippenberg, A hybrid on-chip optomechanical transducer for ultrasensitive force measurements, *Nat. Nanotechnol.* **7**, 509 (2012).
 - [7] N. S. Kampel, R. W. Peterson, R. Fischer, P. L. Yu, K. Cicak, R. W. Simmonds, K. W. Lehnert, and C. A. Regal, Improving Broadband Displacement Detection with Quantum Correlations, *Phys. Rev. X* **7**, 021008 (2017).
 - [8] E. E. Wollman, C. U. Lei, A. J. Weinstein, J. Suh, A. Kronwald, F. Marquardt, A. A. Clerk, and K. C. Schwab, Quantum squeezing of motion in a mechanical resonator, *Science* **349**, 952 (2015).

- [9] J.-M. Pirkkalainen, E. Damskagg, M. Brandt, F. Massel, and M. A. Sillanpaa, Squeezing of Quantum Noise of Motion in a Micromechanical Resonator, *Phys. Rev. Lett.* **115**, 243601 (2015).
- [10] C. U. Lei, A. J. Weinstein, J. Suh, E. E. Wollman, A. Kronwald, F. Marquardt, A. A. Clerk, and K. C. Schwab, Quantum Nondemolition Measurement of a Quantum Squeezed State Beyond the 3 dB Limit, *Phys. Rev. Lett.* **117**, 100801 (2016).
- [11] I. Mahboob, K. Nishiguchi, A. Fujiwara, and H. Yamaguchi, Phonon Lasing in an Electromechanical Resonator, *Phys. Rev. Lett.* **110**, 127202 (2013).
- [12] I. S. Grudin, H. Lee, O. Painter and K. J. Vahala, Phonon Laser Action in a Tunable Two-Level System, *Phys. Rev. Lett.* **104**, 083901 (2010).
- [13] H. Jing, S. K. Ozdemir, X.-Y. Lu, J. Zhang, L. Yang, and F. Nori, \mathcal{PT} -Symmetric Phonon Laser, *Phys. Rev. Lett.* **113**, 053604 (2014).
- [14] H. Lu, S. K. Ozdemir, L. M. Kuang, F. Nori, and H. Jing, Exceptional Points in Random-Defect Phonon Lasers, *Phys. Rev. Appl.* **8**, 044020 (2017).
- [15] F. Massel, T. T. Heikkila, J.-M. Pirkkalainen, S. U. Cho, H. Saloniemi, P. J. Hakonen, and M. A. Sillanpaa, Microwave amplification with nanomechanical resonators, *Nature (London)* **480**, 351 (2011).
- [16] L. M. de Lepinay, E. Damskagg, C. F. Ockeloen-Korppi, and M. A. Sillanpaa, Realization of Directional Amplification in a Microwave Optomechanical Device, *Phys. Rev. Appl.* **11**, 034027 (2019).
- [17] H. Xiong and Y. Wu, Fundamentals and applications of optomechanically induced transparency, *Applied Physics Reviews* **5**, 031305 (2018).
- [18] A. Kronwald and F. Marquardt, Optomechanically Induced Transparency in the Nonlinear Quantum Regime, *Phys. Rev. Lett.* **111**, 133601 (2013).
- [19] G. S. Agarwal and S. Huang, Electromagnetically induced transparency in mechanical effects of light, *Phys. Rev. A* **81**, 041803 (2010).
- [20] S. Weis, R. Riviere, S. Deleglise, E. Gavartin, O. Arcizet, A. Schliesser, and T. J. Kippenberg, Optomechanically induced transparency, *Science* **330**, 1520 (2010).
- [21] M. J. Burek, J. D. Cohen, S. M. Meenehan, N. E. Sawah, C. Chia, T. Ruelle, S. Meesala, J. Rochman, H. A. Atikian, M. Markham, D. J. Twitchen, M. D. Lukin, O. Painter, and M. Loncar, Diamond optomechanical crystals, *Optica* **3**, 1404 (2016).
- [22] J. D. Teufel, D. Li, M. S. Allman, K. Cicak, A. J. Sirois, J. D. Whittaker, and R. W. Simmonds, Circuit cavity electromechanics in the strong-coupling regime, *Nature (London)* **471**, 204 (2011).
- [23] A. H. Safavi-Naeini, T. P. Mayer Alegre, J. Chan, M. Eichenfield, M. Winger, Q. Lin, J. T. Hill, D. E. Chang, and O. Painter, Electromagnetically induced transparency and slow light with optomechanics, *Nature (London)* **472**, 69 (2011).
- [24] M. Karuza, C. Biancofiore, M. Bawaj, C. Molinelli, M. Galassi, R. Natali, P. Tombesi, G. Di Giuseppe, and D. Vitali, Optomechanically induced transparency in a membrane-in-the-middle setup at room temperature, *Phys. Rev. A* **88**, 013804 (2013).
- [25] C. Dong, J. Zhang, V. Fiore, and H. Wang, Optomechanically induced transparency and self-induced oscillations with Bogoliubov mechanical modes, *Optica* **1**, 425 (2014).
- [26] Z. Shen, C.-H. Dong, Y. Chen, Y.-F. Xiao, F.-W. Sun, and G.-C. Guo, Compensation of the Kerr effect for transient optomechanically induced transparency in a silica microsphere, *Opt. Lett.* **41**, 1249 (2016).
- [27] L. Fan, K. Y. Fong, M. Poot, and H. X. Tang, Cascaded optical transparency in multimode-cavity optomechanical systems, *Nat. Commun.* **6**, 5850 (2015).
- [28] Z. Shen, Y.-L. Zhang, Y. Chen, C.-L. Zou, Y.-F. Xiao, X.-B. Zou, F.-W. Sun, G.-C. Guo, and C.-H. Dong, Experimental realization of optomechanically induced non-reciprocity, *Nat. Photonics* **10**, 657 (2016).
- [29] K. Fang, J. Luo, A. Metelmann, M. H. Matheny, F. Marquardt, A. A. Clerk, and O. Painter, Generalized non-reciprocity in an optomechanical circuit via synthetic magnetism and reservoir engineering, *Nat. Phys.* **13**, 465 (2017).
- [30] Z. Shen, Y.-L. Zhang, Y. Chen, F.-W. Sun, X.-B. Zou, G.-C. Guo, C.-L. Zou, and C.-H. Dong, Reconfigurable optomechanical circulator and directional amplifier, *Nat. Commun.* **9**, 1797 (2018).
- [31] H. Lu, Y. Jiang, Y. Z. Wang, and H. Jing, Optomechanically induced transparency in a spinning resonator, *Photonics Res.* **5**, 367 (2017).
- [32] H. Jing, S. K. Ozdemir, Z. Geng, J. Zhang, X.-Y. Lu, B. Peng, L. Yang, and F. Nori, Optomechanically-induced transparency in parity-time-symmetric microresonators, *Sci. Rep.* **5**, 9663 (2015).
- [33] H. Lu, C. Q. Wang, L. Yang, and H. Jing, Optomechanically Induced Transparency at Exceptional Points, *Phys. Rev. Appl.* **10**, 014006 (2018).
- [34] H. Zhang, F. Saif, Y. Jiao, and H. Jing, Loss-induced transparency in optomechanics, *Opt. Express* **26**, 25199 (2018).
- [35] H. Xiong, Y.-M. Huang, L.-L. Wan, and Y. Wu, Vector cavity optomechanics in the parameter configuration of optomechanically induced transparency, *Phys. Rev. A* **94**, 013816 (2016).
- [36] H. Xiong, L.-G. Si, A.-S. Zheng, X. Yang, and Y. Wu, Higher-order sidebands in optomechanically induced transparency, *Phys. Rev. A* **86**, 013815 (2012).
- [37] Y. Jiao, H. Lu, J. Qian, Y. Li, and H. Jing, Nonlinear optomechanics with gain and loss: amplifying higher-order sideband and group delay, *New. J. Phys.* **18**, 083034 (2016).
- [38] Y.-F. Jiao, T.-X. Lu, and H. Jing, Optomechanical second-order sidebands and group delays in a Kerr resonator, *Phys. Rev. A* **97**, 013843 (2018).
- [39] H. Wang, X. Gu, Y. Liu, A. Miranowicz, and F. Nori, Optomechanical analog of two-color electromagnetically induced transparency: Photon transmission through an optomechanical device with a two-level system, *Phys. Rev. A* **90**, 023817 (2014).
- [40] T. Bodiya, V. Sudhir, C. Wipf, N. Smith, A. Buikema, A. Kontos, H. Yu, and N. Mavalvala, Sub-Hertz Optomechanically-Induced Transparency, *arXiv:1812.10184* (2018).
- [41] V. Fiore, Y. Yang, M. C. Kuzyk, R. Barbour, L. Tian, and H. Wang, Storing Optical Information as a Mechanical Excitation in a Silica Optomechanical Resonator, *Phys. Rev. Lett.* **107**, 133601 (2011).
- [42] J. T. Hill, A. H. Safavi-Naeini, J. Chan, and O. Painter, Coherent optical wavelength conversion via cavity op-

- tomemechanics, *Nat. Commun.* **3**, 1196 (2012).
- [43] J. Q. Zhang, Y. Li, M. Feng, and Y. Xu, Precision measurement of electrical charge with optomechanically induced transparency, *Phys. Rev. A* **86**, 053806 (2012).
 - [44] Q. Wang, J. Q. Zhang, P. C. Ma, C. M. Yao, and M. Feng, Precision measurement of the environmental temperature by tunable double optomechanically induced transparency with a squeezed field, *Phys. Rev. A* **91**, 063827 (2015).
 - [45] H. Xiong, Z.-X. Liu, and Y. Wu, Highly sensitive optical sensor for precision measurement of electrical charges based on optomechanically induced difference-sideband generation, *Opt. Lett.* **42**, 3630 (2017).
 - [46] C. Kong, H. Xiong, and Y. Wu, Coulomb-interaction-dependent effect of high-order sideband generation in an optomechanical system, *Phys. Rev. A* **95**, 033820 (2017).
 - [47] H. Xiong, K.-G. Si, and Y. Wu, Precision measurement of electrical charges in an optomechanical system beyond linearized dynamics, *Appl. Phys. Lett.* **110**, 171102 (2017).
 - [48] Y. Guo, K. Li, W. Nie, and Y. Li, Electromagnetically-induced-transparency-like ground-state cooling in a double-cavity optomechanical system, *Phys. Rev. A* **90**, 053841 (2014).
 - [49] T. Ojanen and K. Børkje, Ground-state cooling of mechanical motion in the unresolved sideband regime by use of optomechanically induced transparency, *Phys. Rev. A* **90**, 013824 (2014).
 - [50] Y.-C. Liu, Y.-F. Xiao, X.-S. Luan, and W. C. Wei, Optomechanically-induced-transparency cooling of massive mechanical resonators to the quantum ground state, *Sci. China-Phys. Mech. Astron.* **58**, 050305 (2015).
 - [51] J. Zhang, B. Peng, Ş. K. Özdemir, Y.-X. Liu, H. Jing, X.-Y. Lü, Y.-L. Liu, L. Yang, and F. Nori, Giant nonlinearity via breaking parity-time symmetry: A route to low-threshold phonon diodes, *Phys. Rev. B* **92**, 115407 (2015).
 - [52] K. Totsuka, N. Kobayashi, and M. Tomita, Slow Light in Coupled-Resonator-Induced Transparency, *Phys. Rev. Lett.* **98**, 213904 (2007).
 - [53] J. Zhang, B. Peng, Ş. K. Özdemir, K. Pichler, D. O. Krimer, G. Zhao, F. Nori, Y. Liu, S. Rotter, and L. Yang, A phonon laser operating at an exceptional point, *Nat. Photonics* **12**, 479 (2018).
 - [54] C. Zheng, X. Jiang, S. Hua, L. Chang, G. Li, H. Fan, and M. Xiao, Controllable optical analog to electromagnetically induced transparency in coupled high-Q microtoroid cavities, *Opt. Express* **20**, 18319 (2012).
 - [55] B. Peng, Ş. K. Özdemir, F. Lei, F. Monifi, M. Gianfreda, G. L. Long, S. Fan, F. Nori, C. M. Bender, and L. Yang, Parity-time-symmetric whispering-gallery microcavities, *Nat. Phys.* **10**, 394 (2014).
 - [56] Q. Lin, J. Rosenberg, D. Chang, R. Camacho, M. Eichen, K. J. Vahala, and O. Painter, Coherent mixing of mechanical excitations in nano-optomechanical structures, *Nat. Photonics* **4**, 236 (2010).
 - [57] H. Okamoto, A. Gourgout, C. Y. Chang, K. Onomitsu, I. Mahboob, E. Y. Chang, and H. Yamaguchi, Coherent phonon manipulation in coupled mechanical resonators, *Nat. Phys.* **9**, 480 (2013).
 - [58] M. J. Weaver, F. Buters, F. Luna, H. Eerkens, K. Heeck, S. d. Man, and D. Bouwmeester, Coherent optomechanical state transfer between disparate mechanical resonators, *Nat. Commun.* **8**, 824 (2017).
 - [59] R. Riedinger, A. Wallucks, I. Marinković, C. Löschnauer, M. Aspelmeyer, S. Hong, and S. Gröblacher, Remote quantum entanglement between two micromechanical oscillators, *Nature (London)* **556**, 473 (2018).
 - [60] C. F. Ockeloen-Korppi, E. Damskägg, J. M. Pirkkalainen, M. Asjad, A. A. Clerk, F. Massel, M. J. Wooley, and M. A. Sillanpää, Stabilized entanglement of massive mechanical oscillators, *Nature (London)* **556**, 478 (2018).
 - [61] X.-W. Xu and Y.-J. Li, Antibunching photons in a cavity coupled to an optomechanical system, *J. Phys. B: At. Mol. Opt. Phys.* **46**, 035502 (2013).
 - [62] H. Xie, G.-W. Lin, X. Chen, Z.-H. Chen, and X.-M. Lin, Single-photon nonlinearities in a strongly driven optomechanical system with quadratic coupling, *Phys. Rev. A* **93**, 063860 (2016).
 - [63] H. Xie, C.-G. Liao, X. Shang, M.-Y. Ye, and X.-M. Lin, Phonon blockade in a quadratically coupled optomechanical system, *Phys. Rev. A* **96**, 013861 (2017).
 - [64] L.-L. Zheng, T.-S. Yin, Q. Bin, X.-Y. Lü, and Y. Wu, Single-photon-induced phonon blockade in a hybrid spin-optomechanical system, *Phys. Rev. A* **99**, 013804 (2019).
 - [65] H. Xu, D. Mason, L. Y. Jiang, and J. G. E. Harris, Topological energy transfer in an optomechanical system with exceptional points, *Nature (London)* **537**, 80 (2016).
 - [66] P. Renault, H. Yamaguchi, and I. Mahboob, Virtual Exceptional Points in an Electromechanical System, *Phys. Rev. Appl.* **11**, 024007 (2019).
 - [67] I. Mahboob, H. Okamoto, and H. Yamaguchi, An electromechanical Ising Hamiltonian, *Sci. Adv.* **2**, e1600236 (2016).
 - [68] M. F. Colombano, G. Arregui, N. E. Capuj, A. Piantani, J. Maire, A. Griol, B. Garrido, A. Martinez, C. M. Sotomayor-Torres, and D. Navarro-Urrios, Synchronization of optomechanical cavities by mechanical interaction, *arXiv:1810.06085* (2018).
 - [69] J. P. Mathew, J. D. Pino, and E. Verhagen, Synthetic gauge fields for phonon transport in a nano-optomechanical system, *arXiv:1812.09369* (2018).
 - [70] X.-W. Xu, A.-X. Chen, and Y.-x. Liu, Phononic Josephson oscillation and self-trapping with two-phonon exchange interaction, *Phys. Rev. A* **96**, 023832 (2017).
 - [71] T. Kipf, and G. S. Agarwal, Superradiance and collective gain in multimode optomechanics, *Phys. Rev. A* **90**, 053808 (2014).
 - [72] Q. Bin, X.-Y. Lü, T.-S. Yin, Y. Li, and Y. Wu, Collective radiance effects in the ultrastrong-coupling regime, *Phys. Rev. A* **99**, 033809 (2019).
 - [73] X.-W. Xu, Y.-X. Liu, C.-P. Sun, and Y. Li, Mechanical PT-symmetry in coupled optomechanical systems, *Phys. Rev. A* **92**, 013852 (2015).
 - [74] X. Z. Li, M. C. Kuzyk, and H. Wang, Honeycomb Phononic Networks with Closed Mechanical Subsystems, *arXiv:1901.00561* (2019).
 - [75] F. Massel, S. U. Cho, J. M. Pirkkalainen, P. J. Hakonen, T. T. Heikkilä, and M. A. Sillanpää, Multimode circuit optomechanics near the quantum limit, *Nat. Commun.* **3**, 987 (2012).
 - [76] A. Barfuss, J. Teissier, E. Neu, A. Nunnenkamp, and P. Maletinsky, Strong mechanical driving of a single electron spin, *Nat. Phys.* **11**, 820 (2015).
 - [77] I. Yeo, P. L. de Assis, A. Gloppe, E. Dupont-Ferrier, P. Verlot, N. S. Malik, E. Dupuy, J. Claudon, J. M. Ger-

- ard, A. Auffeves, G. Nogues, S. Seidelin, J. P. Poizat, O. Arcizet, and M. Richard, Strain-mediated coupling in a quantum dot-mechanical oscillator hybrid system, *Nat. Nanotechnol.* **9**, 106 (2014).
- [78] W. Z. Jia, L. F. Wei, Y. Li, and Y.-x. Liu, Phase-dependent optical response properties in an optomechanical system by coherently driving the mechanical resonator, *Phys. Rev. A* **91**, 043843 (2015).
- [79] X.-W. Xu and Y. Li, Controllable optical output fields from an optomechanical system with mechanical driving, *Phys. Rev. A* **92**, 023855 (2015).
- [80] Y. Li, Y. Y. Huang, X. Z. Zhang, and L. Tian, Optical directional amplification in a three-mode optomechanical system, *Opt. Express* **25**, 18907 (2017).
- [81] L.-G. Si, H. Xiong, M. S. Zubairy, and Y. Wu, Optomechanically induced opacity and amplification in a quadratically coupled optomechanical system, *Phys. Rev. A* **95**, 033803 (2017).
- [82] H. Suzuki, E. Brown, and R. Sterling, Nonlinear dynamics of an optomechanical system with a coherent mechanical pump: Second-order sideband generation, *Phys. Rev. A* **92**, 033823 (2015).
- [83] C. Jiang, Y. Cui, Z. Zhai, H. Yu, X. Li, and G. Chen, Tunable slow and fast light in parity-time-symmetric optomechanical systems with phonon pump, *Opt. Express* **22**, 28834 (2018).
- [84] J.-Y. Ma, C. You, L.-G. Si, H. Xiong, J.-H. Li, X.-X. Yang, and Y. Wu, Optomechanically induced transparency in the presence of an external time-harmonic-driving force, *Sci. Rep.* **5**, 11278 (2015).
- [85] L. Tian and P. Zoller, Coupled Ion-Nanomechanical Systems, *Phys. Rev. Lett.* **93**, 266403 (2004).
- [86] W. K. Hensinger, D. W. Utami, H. S. Goan, K. Schwab, C. Monroe, and G. J. Milburn, Ion trap transducers for quantum electromechanical oscillators, *Phys. Rev. A* **72**, 041405(R) (2005).
- [87] P. C. Ma, J. Q. Zhang, Y. Xiao, M. Feng, and Z. M. Zhang, Tunable double optomechanically induced transparency in an optomechanical system, *Phys. Rev. A* **90**, 043825 (2014).
- [88] J. Bochmann, A. Vainsencher, D. D. Awschalom, and A. N. Cleland, Nanomechanical coupling between microwave and optical photons, *Nat. Phys.* **9**, 712 (2013).
- [89] C. Bekker, R. Kalra, C. Baker, and W. P. Bowen, Injection locking of an electro-optomechanical device, *Optica* **4**, 1196 (2017).
- [90] C. W. Gardiner and M. J. Collett, Input and output in damped quantum systems: Quantum stochastic differential equations and the master equation, *Phys. Rev. A* **31**, 3761 (1985).
- [91] D. Malz, L. D. Tóth, N. R. Bernier, A. K. Feofanov, T. J. Kippenberg, and A. Nunnenkamp, Quantum-Limited Directional Amplifiers with Optomechanics, *Phys. Rev. Lett.* **120**, 023601 (2018).
- [92] L. J. Wang, A. Kuzmich, and A. Dogariu, Gain-assisted superluminal light propagation, *Nature (London)* **406**, 277 (2000).
- [93] D. Vitali, S. Gigan, A. Ferreira, H. R. Böhm, P. Tombesi, A. Guerreiro, V. Vedral, A. Zeilinger, and M. Aspelmeyer, Optomechanical Entanglement Between a Movable Mirror and a Cavity Field, *Phys. Rev. Lett.* **98**, 030405 (2007).
- [94] A. Nunnenkamp, K. Børkje, and S. M. Girvin, Single-Photon Optomechanics, *Phys. Rev. Lett.* **107**, 063602 (2011).
- [95] C. Hamsen, K. N. Tolazzi, T. Wilk, and G. Rempe, Strong coupling between photons of two light fields mediated by one atom, *Nat. Phys.* **14**, 885 (2018).
- [96] S.-C. Wu, L.-G. Qin, J. Lu, and Z.-Y. Wang, Phase-dependent double optomechanically induced transparency in a hybrid optomechanical cavity system with coherently mechanical driving, *arXiv:1812.05959* (2018).
- [97] E. X. DeJesus and C. Kaufman, Routh-Hurwitz criterion in the examination of eigenvalues of a system of nonlinear ordinary differential equations, *Phys. Rev. A* **35**, 5288 (1987).